JOURNAL OF BIOMOLECULAR STRUCTURE AND DYNAMICS
https://doi.org/10.1080/07391102.2020.1858164

Depicting the inhibitory potential of polyphenols from *Isatis indigotica* root against the main protease of SARS CoV-2 using computational approaches

Rajesh Ghosh, Ayon Chakraborty, Ashis Biswas and Snehasis Chowdhuri

School of Basic Sciences, Indian Institute of Technology Bhubaneswar, Bhubaneswar, India

Communicated by Ramaswamy H. Sarma

ABSTRACT

The pandemic disease COVID-19, caused by SARS CoV-2, has created a global crisis. Presently, researchers across the globe are in a quest to identify/develop drugs or vaccines by targeting different non-structural proteins (Nsps) of SARS CoV-2. One such important drug target is Nsp5/main protease (Mpro) which plays a critical role in the viral replication. This cysteine protease/Mpro of SARS CoV-2 has high sequence similarity with the same protease from SARS CoV-1. Previously, it has been shown experimentally that eight polyphenols derived from the root of *Isatis indigotica* show inhibitory effect on the cleavage/catalytic activity of the SARS CoV-1 Mpro. But whether these polyphenols exhibit any inhibitory effect on SARS CoV-2 Mpro is unclear. To explore this possibility, here, we have adopted various computational approaches. Polyphenols that qualified the pharmacological parameters (indigo, sinigrin, hesperetin and daidzein) and two well-known Mpro inhibitors (N3 and lopinavir) were subjected to molecular docking studies. Two of them (sinigrin and hesperetin) were selected by comparing their binding affinities with N3 and lopinavir. Sinigrin and hesperetin interacted with the two most important catalytic residues of Mpro (His41 and Cys145). Molecular dynamics studies further revealed that these two Mpro-polyphenol complexes are more stable and experience less conformational fluctuations than Mpro-N3/lopinavir complex. The Mpro-hesperetin complex was more compact and less expanded than Mpro-sinigrin complex. These findings were additionally validated by MM-GBSA analysis. As a whole, our study revealed that these two polyphenols may be potent SARS CoV-2 Mpro inhibitors and may possibly be considered for COVID-19 treatment.

ARTICLE HISTORY
Received 23 August 2020
Accepted 15 November 2020

KEYWORDS
COVID-19; SARS CoV-2 main protease; docking; molecular dynamics simulation; *Isatis indigotica* polyphenols

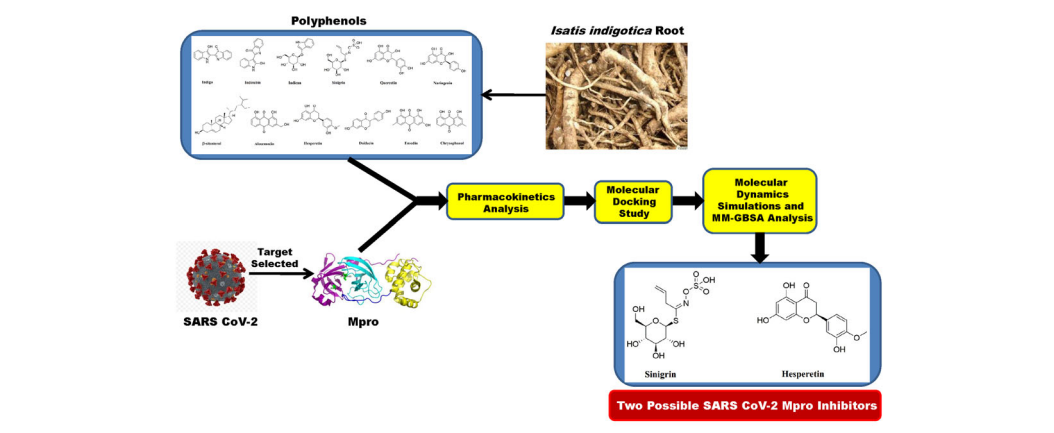

Abbreviations: COVID-19: Corona virus disease 2019; SARS CoV-2: Severe acute respiratory syndrome corona virus-2; Nsps: Non-structural proteins; Mpro: Main protease; MD: Molecular dynamics; RMSD: Root mean square deviation; RMSF: Root mean square fluctuation; Rg: Radius of gyration; SASA: Solvent accessible surface area

1. Introduction

The world is facing a pandemic situation due to the outbreak of COVID-19 disease which is caused by the pathogen severe acute respiratory syndrome coronavirus-2 (SARS CoV-2). It is a zoonotic virus that spread rapidly from China to many countries around the world (Zhu et al., 2020). So far, SARS

CONTACT Ashis Biswas abiswas@iitbbs.ac.in; Snehasis Chowdhuri snehasis@iitbbs.ac.in School of Basic Sciences, Indian Institute of Technology Bhubaneswar, Bhubaneswar, Odisha 752050, India

CoV-2 has infected almost twenty-three million people worldwide, causing approximately 800,000 deaths as on 22nd August 2020, (https://www.worldometers.info/coronavirus/). SARS CoV-2 mostly affects the lower respiratory tract, which causes pneumonia (N. Chen et al., 2020; Ren et al., 2020; Zhu et al., 2020). This virus also affects the gastrointestinal system, kidney, heart and central nervous system, with the common symptoms including fever, cough and diarrhea (N. Chen et al., 2020; Ren et al., 2020; Zhu et al., 2020). SARS CoV-2 is an enveloped, positive-sense, single-stranded RNA virus that belongs to the β-lineage of the coronavirus (Zheng, 2020). The β-lineage also contains two other important human pathogens, the SARS CoV-1 and MERS CoV. Toyoshima *et al*. reported that the mortality rate of SARS CoV-2 (6.6%) is lower than that of SARS CoV-1 (9.6%) and MERS CoV (34.3%) (Toyoshima et al., 2020). However, current data indicates that SARS CoV-2 is more contagious and has a larger basic reproductive number (R_0) value than SARS CoV-1 and MERS CoV, resulting in a higher overall death toll than SARS CoV-1 and MERS CoV (Sanche et al., 2020; Tang et al., 2020).

No approved therapeutic/effective treatment is currently available to combat this outbreak. Thus, search for appropriate drugs and suitable vaccines are highly in demand to control COVID-19. The SARS CoV-2 genome is composed of a 29.9 bps long RNA strand. When this coronavirus infects a host cell, it acts as a messenger RNA (mRNA). This mRNA directs the synthesis of polyproteins required for the multiplication of new viruses. Mainly two cysteine proteases [the main protease (Mpro) and papain-like protease (PLpro)] are responsible for the processing of viral polyproteins at a specific site into functional units for virus replication (Fan et al., 2004; Rota et al., 2003). Mpro helps in the proteolytic cleavage at 11 sites involving the Leu-Gln↓(Ser, Ala, Gly) sequence of the viral polyprotein and resulting in the release of a total number of 16 nonstructural proteins (Nsps) (Fan et al., 2004; Rota et al., 2003). The Mpro from SARS CoV-2 is reported to share more than 96% sequence similarity with the same protease from SARS CoV-1 and MERS which makes it an ideal target for broad-spectrum anti-CoV therapy (Ghosh et al., 2020b). Even higher sequence similarity is observed between the main protease from SARS CoV-1 and SARS CoV-2 with a difference in only twelve amino acid residues (Figure 1) (Macchiagodena et al., 2020).

Each of the protomers of the homodimeric SARS CoV-2 Mpro protein consists of three domains: domain I (amino acid residues 8-101), domain II (amino acid residues 102-184) and domain III (amino acid residues 201-303) (Figure 1) (Jin et al., 2020). Domain I and II are mainly β-barrels, while, domain III consists mainly of α-helices (Jin et al., 2020). The catalytic site/active site/substrate binding site comprises of cysteine (Cys145) and histidine (His41) amino acid moiety and is located at the cleft of domain I and domain II (Jin et al., 2020). Cysteine145 serves as a common nucleophile and plays a vital role in the proteolytic functioning of Mpro (Anand et al., 2003; Chou et al., 2003; Hsu et al., 2005). Since the proteolytic processing is the functional significance of Mpro in viral propagation, this unique property makes this protease an important drug target. Besides this, lack of any human homolog of Mpro makes it an ideal target for the development of drugs against COVID-19 infection (Y. Kim et al., 2016). Many studies have been carried out recently to find suitable inhibitors of Mpro using drug repurposing strategy (Arun et al., 2020; Elmezayen et al., 2020; Kandeel & Al-Nazawi, 2020; Khan et al., 2020; Mahanta et al., 2020; Muralidharan et al., 2020). Furthermore, various phytochemicals are also proposed as the SARS CoV-2 main protease inhibitors through screening and structure-based design approach (Aanouz et al., 2020; Borkotoky & Banerjee, 2020; Enmozhi et al., 2020; Gyebi et al., 2020; Islam et al., 2020; Joshi et al., 2020; Umesh et al., 2020). In recent times, it has been found that plant-derived polyphenols can serve as potent SARS CoV-2 Mpro inhibitors. Our group has identified three polyphenols from green tea [epigallocatechin gallate (EGCG), epicatechingallate (ECG) and gallocatechin-3-gallate (GCG)] can inhibit the catalytic activity of Mpro (Ghosh et al., 2020a). In another independent study, we have identified six polyphenols from *Broussonetia papyrifera* which have the potency to inhibit the proteolytic activity SARS CoV-2 Mpro (Ghosh et al., 2020b). Purohit and coworkers have found that polyphenols such as oolonghomobisflavan-A and theaflavin-3-O-gallate from the tea plant (*Camellia sinensis L.*) can act as effective SARS CoV-2 Mpro inhibitors (Bhardwaj et al., 2020). Apart from these, other polyphenols have also been reported to show inhibition of Mpro activity in SARS CoV-2 (S. Das et al., 2020). The roots of *Isatis indigotica*, contains mainly twelve polyphenols (indigo, indirubin, indican, sinigrin, quercetin, naringenin, β-sitosterol, aloeemodin, hesperetin, daidzein, emodin and chrysophanol) (Figure 2) (Lin et al., 2005). Different polyphenolic compounds from the root extract of *I. indigotica* have also been reported to exhibit antiviral activity against a wide range of viruses like influenza-A virus, rabies virus, Japanese Encephalitis Virus and human immunodeficiency virus (HIV) (Chang et al., 2012; Heredia et al., 2005; Hertel et al., 2007; Hsuan et al., 2009; Ko et al., 2006; Mak et al., 2004; Zou & Koh, 2007). Some of them have even shown antiviral effects against poliovirus, vesicular stomatitis virus, sindbis virus, herpes simplex virus types 1 and 2, parainfluenza virus, and vaccinia virus (Andersen et al., 1991; H. K. Kim et al., 2001; Paredes et al., 2003; Semple et al., 2001).

Additionally, Chao and colleagues have shown anti-SARS CoV-1 main protease activity of some of these polyphenols derived from the root of *Isatis indigotica* (Lin et al., 2005). They evaluated the inhibitory activity of these polyphenolic compounds by utilizing both cell-free and cell-based cleavage assays. Among all of the polyphenols (mentioned in Figure 2), quercetin, naringenin, emodin, and chrysophanol did not show any inhibitory effects on the SARS CoV-1 Mpro. The polyphenols indigo, sinigrin, β-sitosterol, aloeemodin and hesperetin showed the evidence of inhibitory effect with an IC50 value in the range of 2.5-502.1 μg/ml based on the cell-based cleavage activity of the SARS CoV-1 main protease. On the other hand, cell-free cleavage activity confirmed the inhibitory effect of eight polyphenols from *I. indigotica* (indigo, indirubin, indican, sinigrin, β-sitosterol, aloeemodin, hesperetin and daidzein) towards the SARS CoV-1 Mpro with an IC50 value ranging from 18.1- 81.3 μg/ml. But whether

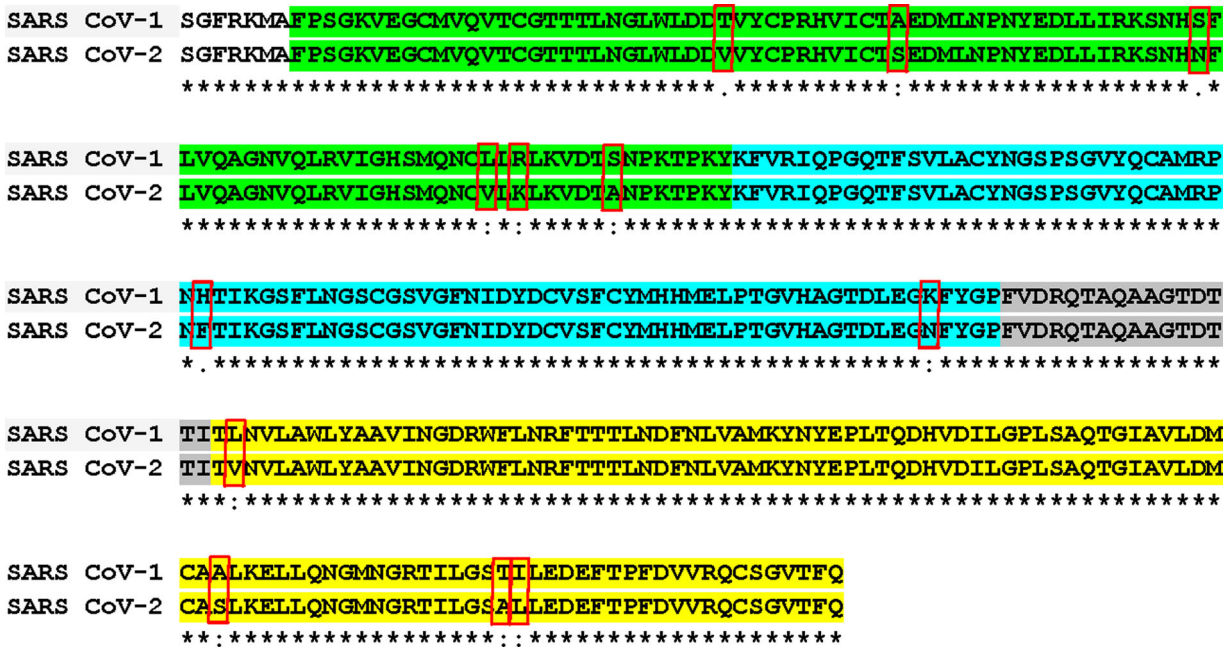

Figure 1. Sequence alignment of the main protease (Mpro) from SARS CoV-1 and SARS CoV-2 (Tahir UI Qamar et al., 2020). The amino acid sequence alignment of Mpro from SARS CoV-1 (PDB ID 1UJ1) and SARS CoV-2 (PDB ID 6LU7) was performed using CLUSTALW (1.83) multiple sequence alignment program. The main protease from the two coronaviruses possesses Domain I (highlighted with green), Domain II (highlighted with turquoise), Domain III (highlighted in yellow) and a connecting loop (highlighted with grey). The symbols represent identical residues (*), conserved substitutions (:) and semi-conserved substitutions (.), respectively. The different amino acid residues are shown inside red-colored rectangular boxes.

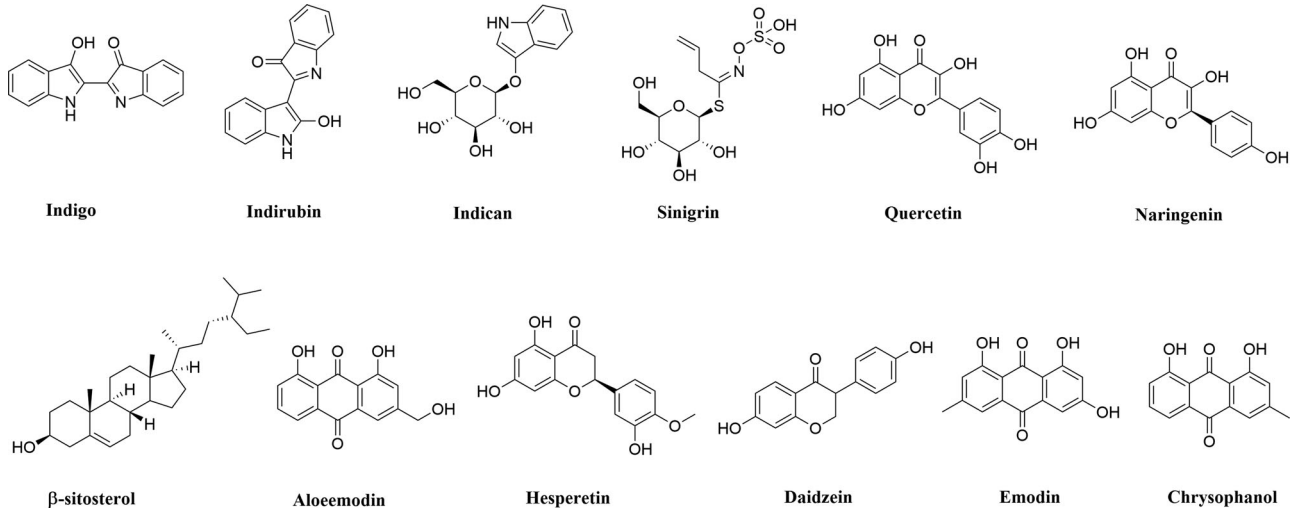

Figure 2. Chemical structure of *I. indigotica* polyphenols. The two-dimensional structures of twelve polyphenols from *I. indigotica* with their respective names are shown.

these eight polyphenols which possess SARS CoV-1 Mpro inhibitory activity, can also exhibit any antiviral activity against SARS CoV-2 by inhibiting the catalytic/proteolytic activity of Mpro is not clear till now. Therefore, in this study, we have examined the inhibitory efficiency of these eight polyphenols (indigo, indirubin, indican, sinigrin, β-sitosterol, aloeemodin, hesperetin and daidzein) from *I. indigotica* against SARS CoV-2 Mpro with the aid of *in-silico* docking studies, molecular dynamics simulations and MM-GBSA analysis. This study has revealed that two polyphenols of *I. indigotica* (sinigrin and hesperetin) have a stronger binding affinity towards Mpro and may possibly act as inhibitors for the SARS CoV-2 Mpro.

2. Materials and methods

2.1. Preparation of Mpro

The SARS CoV-2 Mpro crystal structure was retrieved from the RCSB Protein Data Bank (http://www.rcsb.org) (PDB ID: 6LU7) (Jin et al., 2020). Then, the presence of improper bonds, missing hydrogens, side-chain anomalies were checked and corrected accordingly. After correcting all those aspects, the structure file was inserted into AutoDock Tools and regular procedures were followed to get pdbqt file format of Mpro (Morris et al., 2008; 2009).

2.2. Preparation of the ligands

Each of the structures of *Isatis indigotica* polyphenols was retrieved from PubChem database server in MDL/SDF format (https://pubchem.ncbi.nlm.nih.gov). Then B3LYP/6-31G* basis set in *Gaussian09* software was used for the optimization of each of the *I. indigotica* polyphenol structures (Frisch et al., 2009). These ligands were then prepared using the AutoDock Tools involving the addition of hydrogen followed by assignment of the appropriate ionization state of each of the ligands and regular processes were used in AutoDock Tools to obtain the pdbqt files for *I. indigotica* polyphenols.

2.3. Molecular docking

We have used AutoDock Vina for the entire docking calculations of Mpro with N3, lopinavir and *I. indigotica* polyphenols where the grid box with a 10.0 Å radius throughout the active site region was chosen (Morris et al., 2008, 2009). The lowest root mean square deviation (RMSD), and the highest Vina score conformations of each complex were selected. The output from AutoDock Vina was rendered with DS visualizer software (Biovia, 2017).

2.4. Molecular dynamics simulation

We have performed molecular dynamics (MD) simulations of unligated Mpro, Mpro-sinigrin, Mpro-hesperetin, Mpro-N3 and Mpro-lopinavir complexes using the GROMACS 2019 (Abraham et al., 2015). We have used the GROMOS9653a6 force field and SPC water model for all the simulations, where the PRODRG server was used for the ligand topologies (Oostenbrink et al., 2004; Schuttelkopf & van Aalten, 2004). The LINCS algorithm was used to constrain all the bond lengths of protein and N3/lopinavir/*I. indigotica* polyphenols, while for restraining water molecules we have used SETTLE algorithm (Hess et al., 1997; Miyamoto & Kollman, 1992). A total number of 30226, 30205, 30208, 30198, 30196 water molecules containing the unligated Mpro, Mpro-sinigrin, Mpro-hesperetin, Mpro-N3 and Mpro-lopinavir complexes, respectively, were placed in a cubic box system. Each system was energy-minimized using the steepest descent algorithm and equilibrated to achieve the appropriate volume. The leapfrog algorithm with time step 2 fs was used and at every 5 steps, the neighbour list was updated. Long-range electrostatics were calculated using the Particle Mesh Ewald method with cut off 1.2 nm and a Fourier grid spacing of 1.2 nm (Essmann et al., 1995). The periodic boundary conditions were applied and the equilibration of the systems was carried out mainly in two stages. First, the system was equilibrated at 300 K in the NVT ensemble using the v-rescale algorithm for 10 ns. Then the system was further equilibrated in the NPT ensemble for 10 ns by positional restraining of the complexes (unligated Mpro, Mpro-N3, Mpro-lopinavir and Mpro-*I. indigotica* polyphenol complexes). The Parrinello-Rahman method and Berendsen barostat were employed to maintain the pressure and temperature, respectively (Berendsen et al., 1984; Parrinello & Rahman, 1981). For each system, the average temperature and pressure values remained close to the desired values. The equilibrated systems were then subjected to unrestrained production MD simulations for 100 ns each, maintaining target pressure (1 bar) and temperature (300 K). Finally, we have used the MD trajectories for each system to calculate some important parameters in order to check the protein-ligand interactions, namely, root mean square deviation (RMSD), root mean square fluctuation (RMSF), the radius of gyration (Rg), and solvent accessible surface area (SASA) (Ghosh et al., 2020a, 2020b).

2.5. MM-GBSA analysis

Recently, for calculating the binding free energies of ligands to the receptor, several implicit solvent models have been used such as a) the Molecular Mechanics Generalized Born Surface Area (MM-GBSA) b) Molecular Mechanics Poisson-Boltzmann Surface Area (MM-PBSA) and c) Free energy perturbation etc (Jianzhong Chen, 2016; J. Chen et al., 2015; B. K. Das et al., 2019; Hou et al., 2011). Here, we have used the MM-GBSA method to calculate the relative binding free energies of N3, lopinavir and *I. indigotica* polyphenols to Mpro. The free energy of binding can be calculated as $\Delta G_{bind} = E_{complex} - (E_{ligand} + E_{receptor})$, where, ΔG_{bind} is the energy difference between the complex and sum of the energies of the receptor and ligand. The energy for complex ($E_{complex}$), receptor ($E_{receptor}$) and ligand (E_{ligand}) can be further divided into molecular mechanics (electrostatic and van der Waals) and solvation (polar and non-polar) components, $E_{Total} = E_{MM} + E_{Sol}$.

Prime MM-GBSA uses the VSGB 2.0 implicit solvation model to estimate the binding energy of the receptor-ligand complex. The generalized Born model with an external dielectric constant of 80 and an internal dielectric constant of 1is used for the estimation of the polar contribution of the free energy, while the non-polar energy contribution is calculated from the solvent-accessible surface area (SASA). The prime module of the Schrodinger suite (Schrödinger Release 2020-1: Prime, Schrödinger, LLC, New York, NY, 2020) was used for all MM-GBSA calculations.

2.6. Pharmacokinetic properties analysis

SwissADME and pkCSM-pharmacokinetics online softwares were used for the prediction of different pharmacokinetic properties of polyphenols from *I. indigotica* (Daina et al., 2017; Pires et al., 2015). Levels of toxicity along with the drug-likeness properties of these polyphenols such as absorption, distribution, metabolism and excretion parameters were mainly scrutinized.

3. Result and discussion

Jin *et al* first resolved the crystal structure of Mpro in complex with a Michael inhibitor N3 (Jin et al., 2020). The three-dimensional structure of Mpro in this co-crystal revealed that N3 binds irreversibly to the Cys-His catalytic dyad of Mpro. In

Table 1. Pharmacokinetic properties of *Isatis indigotica* polyphenols.

Compound	MW	H-Ac	H-Do	Nrot	TPSA	LogP	IA	TC	LD50	HT	AT	MTD	NLV
Indigo	262.26	3	2	1	65.45	3.19	91.929	0.334	2.035	No	No	0.132	0
Indirubin	262.26	3	2	1	65.45	3.19	91.285	0.339	2.378	No	No	−0.428	0
Indican	295.29	6	5	3	115.17	−0.6534	50.586	0.354	2.063	Yes	No	0.766	0
Sinigrin	359.37	10	5	7	199.79	−1.7715	0	0.503	1.875	No	No	1.327	0
β-sitosterol	414.71	1	1	6	20.23	8.0248	94.464	0.628	2.552	No	No	−0.621	1
Aloeemodin	270.24	5	3	1	94.83	1.3655	74.179	0.008	2.329	No	Yes	−0.089	0
Hesperetin	302.28	6	3	2	96.22	2.5185	70.277	0.044	2.042	No	No	0.25	0
Daidzein	254.24	4	2	1	70.67	2.8712	94.839	0.164	2.164	No	No	0.187	0

MW = Molecular weight (g/mol); H-Ac = No. of hydrogen bond acceptors; H-Do = No. of hydrogen bond donors; Nrot = No. of rotatable bonds; TPSA = Topological polar surface area (Å^2); LogP = Predicted octanol/water partition coefficient; IA = Intestinal absorption (% Absorbed); TC = Total clearance (log ml/min/kg); LD50 = Oral rat acute toxicity (mol/kg); HT = Hepatoxicity; AT = AMES toxicity; MTD = Maximum tolerated dose for human (log mg/kg/day); NLV = No. of Lipinski rule violations.

Table 2. The binding energy of N3, lopinavir and different polyphenols of *I. indigotica* with the active site of SARS CoV-2 Mpro.

Drug	Binding energy (kcal/mol)
N3	−7.0
Lopinavir	−7.3
Daidzein	−6.5
Indigo	−6.8
Sinigrin	−7.8
Hesperetin	−7.9

the same paper, Yang and coworkers estimated the enzymatic activity of Mpro in the absence and presence of N3 using a fluorescence-based assay (Jin et al., 2020). This experiment clearly suggested that N3 inhibits the proteolytic activity of Mpro. Thus, many investigators including us have chosen N3 as a standard substrate and compared the binding affinity and/or binding modes between various small molecules including green tea polyphenols with that of 'Mpro-N3 complex' (Ghosh et al., 2020a; Odhar et al., 2020). In our previous report, we have demonstrated that N3 interacts with both of the catalytic residues (His41 and Cys145) of Mpro with a binding affinity of −7.0 kcal/mol (Ghosh et al., 2020a). Besides N3, many anti-HIV drugs also have a good binding affinity towards the active site of Mpro (Beck et al., 2020). One such anti-HIV drug is lopinavir. In the recent past, lopinavir has been taken as a standard Mpro inhibitor by us and many other investigators (Bhardwaj et al., 2020; S. Das et al., 2020; Ghosh et al., 2020b; Gyebi et al., 2020). Thus, we have decided to take these two compounds (N3 and lopinavir) as standard inhibitors for this study. We also decided to screen the polyphenols (indigo, indirubin, indican, sinigrin, β-sitosterol, aloeemodin, hesperetin and daidzein) of *Isatis indigotica* with the aid of pharmacokinetic analysis before assessing their binding propensity towards Mpro.

3.1. Screening of polyphenols of isatis indigotica using pharmacokinetics analysis

Understanding the pharmacokinetics behavior of a particular compound is extremely essential for assessing its suitability towards human administration. Pharmacokinetics properties obtained from SwissADME and pkCSM-pharmacokinetics tools are listed in Table 1.

The molecular weight of all eight polyphenols ranged between ∼254 to ∼414 g/mol (<500 g/mol). Thus, their transportation, diffusion and absorption inside the body should be easier. All polyphenols (except β-sitosterol) obeys the Lipinski's rule. Their TPSA values were less than 200 Å^2 (20-199 Å^2) which indicates their good bioavailability. Among these eight polyphenols, indican had shown hepatotoxicity and aloeemodin is an AMES positive compound. A positive AMES test indicated that aloeemodin is mutagenic and may act as a carcinogen. Pharmacokinetics analysis also pointed towards an unfavorable (negative) tolerance dose of aloeemodin. Such unfavorable tolerance dose was also observed for indirubin and β-sitosterol which ruled out the possibility of their usage as potential drugs for humans. The other four polyphenols (indigo, sinigrin, hesperetin and daidzein) are non-toxic and satisfy all drug-likeness rules. Therefore, these four polyphenols were selected for examining their binding propensity towards SARS CoV-2 Mpro using molecular docking studies.

3.2. Assessment of binding affinity and binding modes of different polyphenols using molecular docking studies

N3, lopinavir and polyphenols of *Isatis indigotica* possessing favorable drug-likeness characteristics were docked to assess the polyphenol(s) exhibiting higher or comparable binding energy to that of 'Mpro-N3/lopinavir interaction'. The binding energy of N3 and lopinavir towards Mpro was −7.0 and −7.3 kcal/mol, respectively (Table 2) (Ghosh et al., 2020a, 2020b).

We also estimated the binding energy of four polyphenols (indigo, sinigrin, hesperetin and daidzein) towards Mpro using molecular docking studies. It was found that the binding energy of daidzein and indigo (-6.5 and −6.8 kcal/mol, respectively) was lower in comparison to the standards, N3 and lopinavir (Table 2). On the contrary, the other two polyphenols (sinigrin and hesperetin) exhibited higher binding affinity (-7.8 to −7.9 kcal/mol) towards Mpro compared to that of N3 and lopinavir (Table 2). As sinigrin and hesperetin had higher binding affinity than N3 and lopinavir, we decided to proceed further with these two polyphenols.

The amino acid residues within the active site of Mpro which were interacting with these two selected polyphenols were carefully examined with the aid of discovery studio visualizer. It was evidenced that sinigrin and hesperetin efficiently interacted with different amino acid residues of domain I and II of Mpro (Figure 3). When sinigrin was docked into the active site of Mpro, six hydrogen bond interactions [His41 (2.55 Å), Tyr54 (2.35 Å), Leu141 (2.50 Å), Ser144 (2.41 Å),

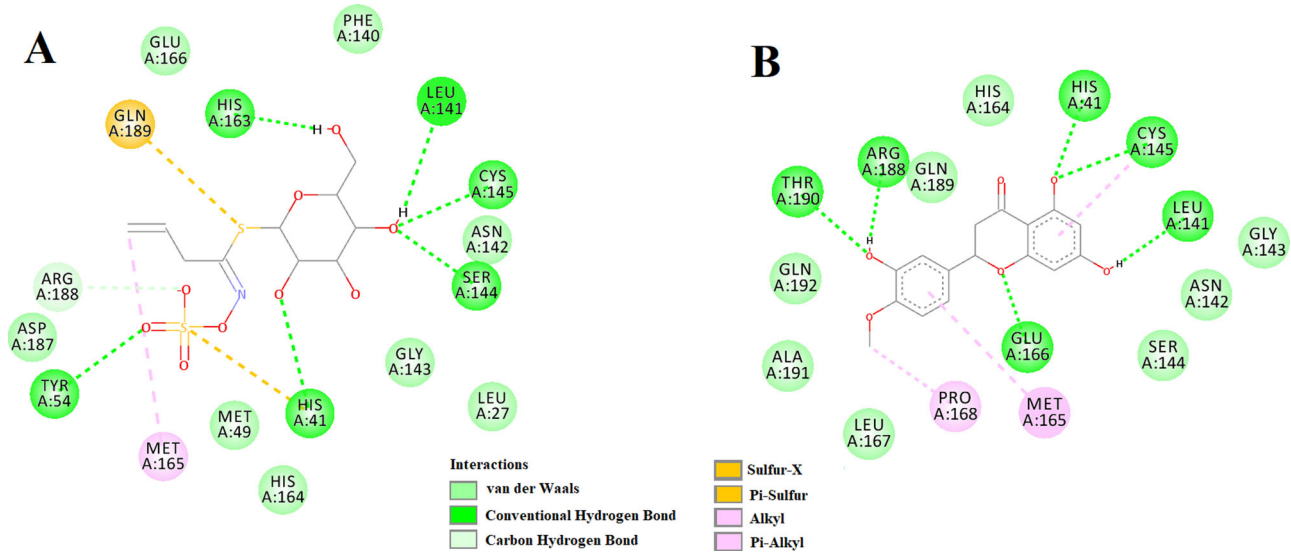

Figure 3. Molecular docking of two *I. indigotica* polyphenols (sinigrin and hesperetin) with Mpro. The docked conformation of the Mpro-sinigrin complex (A) and Mpro-hesperetin complex (B) depicting the possible interactions with various amino acids of Mpro. Both of them interact with various amino acid residues including His41 and Cys145 of Mpro.

Cys145 (2.42 Å) and His163 (2.31 Å)], eight van der Waals interactions (Leu27, Met49, Phe140 Asn142, Gly143, His164, Glu166 and Asp187) and one C-H bond interaction (Arg188) were evidenced (Figure 3A). Besides these, one sulfur-X (Gln189), multiple π-alkyl (His41 and His163) and one alkyl (Met165) interactions were observed in the Mpro-sinigrin complex (Figure 3A). Interestingly, a similar number of H-bond interactions (6 nos) were observed when hesperetin was docked to the active site of Mpro. Hesperetin formed a single hydrogen bond with His41 (2.32 Å), Leu141 (2.32 Å), Cys145 (2.31 Å), Glu166 (2.30 Å), Arg188 (2.31 Å) and Thr190 (2.32 Å) of Mpro (Figure 3B). Mpro-hesperetin complex was further stabilized by one alkyl (Pro168), eight van der Waals interactions (Asn142, Gly143, Ser144, His164, Leu167, Ala191, Gln189 and Gln192) and one π-alkyl (Met165) interaction (Figure 3B). Even, the interaction of two selected standards (N3 and lopinavir) with several critical residues within the active site of Mpro was well-evidenced in our previous studies (Ghosh et al., 2020a, 2020b). The Mpro-N3 complex was stabilized by multiple hydrogen bond interactions (especially with His41 and Cys145 of Mpro) and many other non-covalent interactions (Ghosh et al., 2020a). We also observed that Cys145, Met49 and Pro168 of Mpro interacted with lopinavir via hydrogen bond, π-sulfur bond and alkyl bond, respectively (Ghosh et al., 2020b). Lopinavir also formed numerous van der Waals interactions with various amino acid residues (Thr25, Thr26, Leu141, Tyr54, Phe140, Asn142, Gly143, His163, His164, Met165, Glu166, Leu167, Asp187, Arg188, Gln189, Thr190 and Gln192) of Mpro (Ghosh et al., 2020b). Altogether, molecular docking studies clearly revealed that the two selected polyphenols (sinigrin and hesperetin) interacted with two key residues (His41 and Cys145) of Mpro via hydrogen bond interactions (Figure 3). Even, their binding affinity towards Mpro was more than that of the binding affinity of N3/lopinavir to Mpro (Table 2). Thus, it can be concluded that sinigrin and hesperetin may possibly inhibit the proteolytic activity of Mpro and may potentially be used to treat patients with COVID-19.

These two Mpro-polyphenol complexes were further subjected to molecular dynamics simulations as well as binding free energy computations to assess the stability of these complexes.

3.3. Molecular dynamics simulation studies

MD simulations were performed for 100 ns using GROMOS9653a6 force field. Prior to investigating different structural properties like overall complex stability (RMSD), conformational fluctuations (RMSF), structural compactness (Rg), and solvent accessibility (SASA), we determined the binding modes present in Mpro-sinigrin and Mpro-hesperetin complex after the completion of MD run. One π-alkyl interaction (Met165), eight van der Waals interactions (Met49, Asn142, Gly143, Ser144, His164, Glu166, His172 and Gln189), two C-H bond interactions (Asp187 and Arg188) and five hydrogen bond interactions [His41 (2.5Đ), Phe140 (2.4Đ), Leu141 (2.5Đ), Cys145 (2.5Đ) and His163 (2.5Đ)] were evidenced in Mpro-sinigrin system (Figure 4). On the other hand, one π-sulfur interaction (Met165), eight van der Waals interactions (Pro52, Tyr54, Glu166, Leu167, Asp187, Arg188, Ala191 and Gln192), one π-π interaction (His41) and five hydrogen bond interactions [Cys145 (2.4Đ), His164 (2.3Đ), Pro168 (2.4Đ), Gln189 (2.5Đ) and Thr190 (2.4Đ)] were evidenced in Mpro-hesperetin complex (Figure 4). Both polyphenols (sinigrin and hesperetin) had most of the intermolecular hydrogen bonding with Mpro between 1 to 6 throughout the whole simulation process with an average value of 4 (Figure 5). It was clearly evident from this analysis that the interaction of these two polyphenols with many important amino acid residues (including His41 and Cys145) of Mpro remained intact even after the MD simulation. These findings affirmed the stability of these complexes as well as

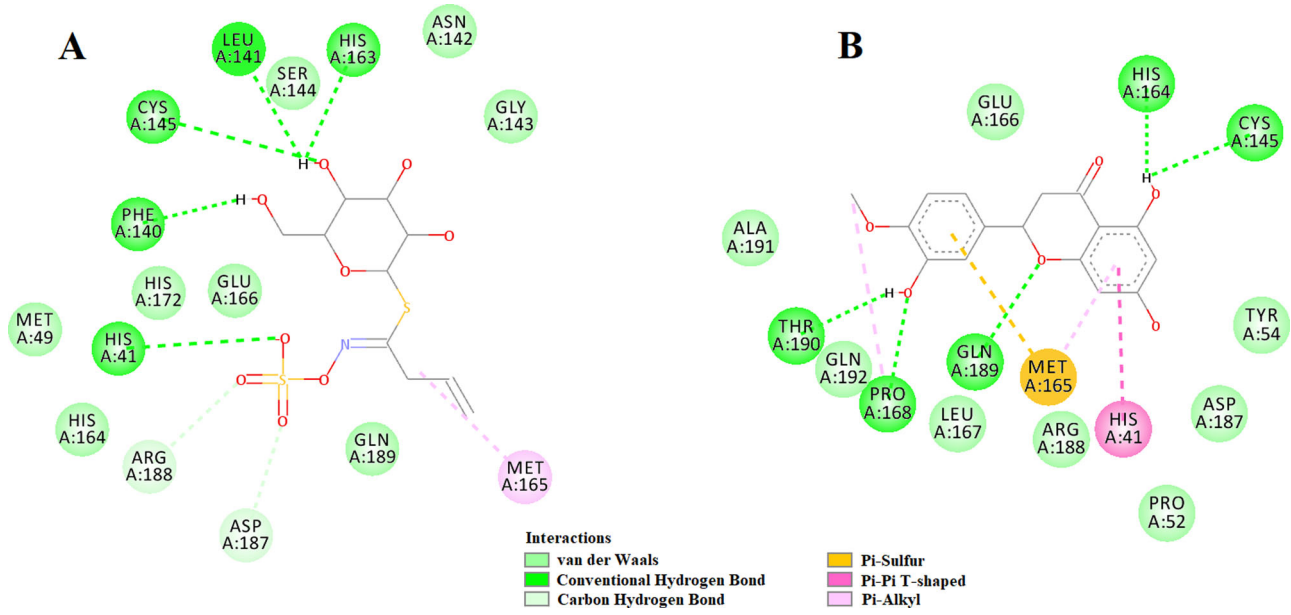

Figure 4. Identification of binding residues/modes within Mpro-sinigrin and Mpro-hesperetin complex after MD run. The docked conformation of the Mpro-sinigrin complex (A) and Mpro-hesperetin complex (B) depicting the possible interactions with various amino acids of Mpro after 100 ns MD run. Both these polyphenols are shown to interact with His41 and Cys145 of Mpro.

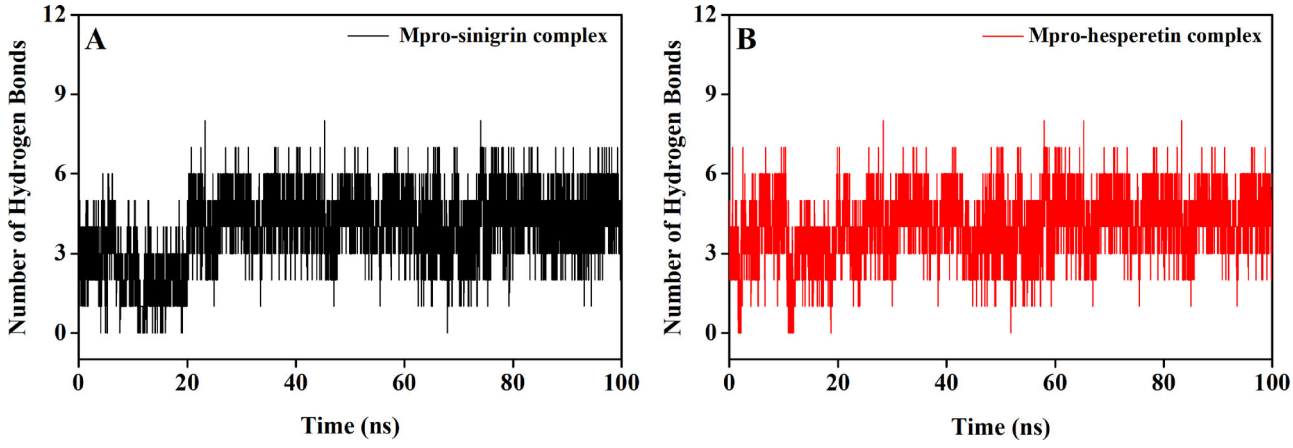

Figure 5. Hydrogen bond profiles of Mpro complexed with *I. indigotica* polyphenols. The hydrogen bond profiles of Mpro-sinigrin complex and Mpro-hesperetin complex throughout the 100 ns of MD run are plotted in A and B, respectively.

strengthened their candidatures as SARS CoV-2 Mpro inhibitors.

3.3.1. RMSD and RMSF analysis

To revalidate the stability of Mpro-sinigrin and Mpro-hesperetin complex, we estimated the RMSD of backbone alpha carbon atoms of these two systems and compared the same with that of three other systems (unligated Mpro, Mpro-N3 and Mpro-lopinavir) (Figure 6). For unligated Mpro, the RMSD value from 2 ns to 17 ns maintained a constant value (~0.21-0.22 nm). The value increased progressively and reached to ~0.31 nm (with some fluctuations) at 65 ns and remained almost the same till the end of the MD run (Figure 6A and B) (Ghosh et al., 2020b). The RMSD value of Mpro-N3 complex was ~0.18 nm at 2 ns, which rose to ~0.28 nm at 10 ns. The RMSD magnitude remained the same upto 25 ns. Then, with the next 6 ns, the value was slightly decreased (~0.26 nm) and persisted at the same value till 100 ns (Figure 6A). The RMSD values for Mpro-lopinavir complexes were found to remain almost constant (~0.36-0.37 nm) from 10 ns to 100 ns with some marginal fluctuations (Figure 4A) (Ghosh et al., 2020b). On the other hand, the magnitude of RMSD corresponding to Mpro-sinigrin and Mpro- hesperetin complexes attained an equilibrium value after 20 ns (~0.23 nm) and remained almost the same throughout the 100 ns simulation (Figure 6B). The average RMSD values of unligated Mpro, Mpro-N3, Mpro-lopinavir, Mpro-sinigrin and Mpro-hesperetin complexes were 0.309 nm, 0.259 nm, 0.371 nm, 0.234 nm, 0.229 nm, respectively (Table 3). These results suggested that Mpro-sinigrin and Mpro-hesperetin complexes were relatively more stable than that of Mpro-N3/Mpro-lopinavir complexes.

To find out the conformational flexibility of unligated Mpro and other Mpro-complexes, we have calculated the RMSF of alpha carbon atoms for all systems (Figure 7). It was quite evident from the RMSF profiles that the Mpro-lopinavir system experiences more conformational fluctuations in

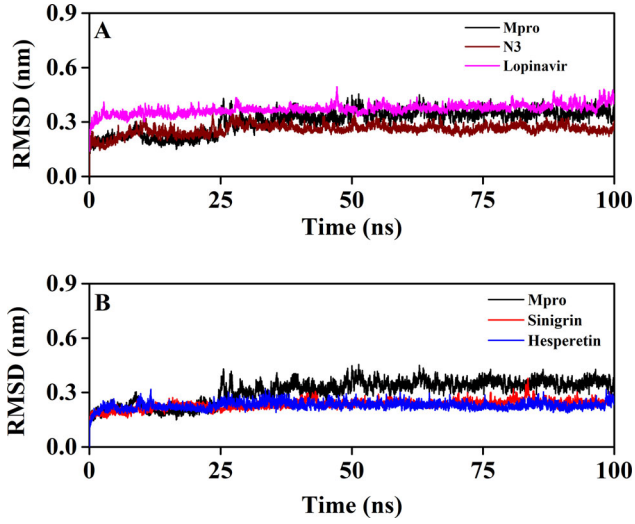

Figure 6. The RMSD plots of unligated Mpro, Mpro-N3, Mpro-lopinavir and two Mpro-polyphenols complexes. The RMSD plots of unligated Mpro, Mpro-N3 and Mpro-lopinavir systems are plotted in A while B represents the RMSD plots of unligated Mpro, Mpro-sinigrin complex and Mpro-hesperetin complex. The MD simulations for each system were performed for 100 ns.

Table 3. Average values of the RMSD and RMSF for the simulated systems.

System	RMSD (nm)	RMSF (nm)
Unligated Mpro	0.309	0.1937
Mpro-N3	0.259	0.1575
Mpro-lopinavir	0.371	0.1948
Mpro-sinigrin	0.234	0.1309
Mpro-hesperetin	0.229	0.1227

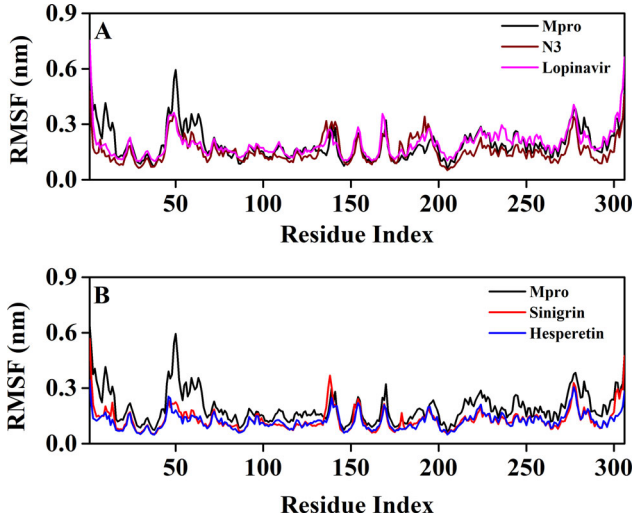

Figure 7. RMSF profiles of unligated Mpro and Mpro complexed with two selected standards and *I. indigotica* polyphenols. The RMSF values of unligated Mpro, Mpro-N3 and Mpro-lopinavir complexes are plotted in A against the amino acid residues of Mpro. B represents the RMSF plots of unligated Mpro, Mpro-sinigrin complex and Mpro-hesperetin complex against the amino acid residues of Mpro.

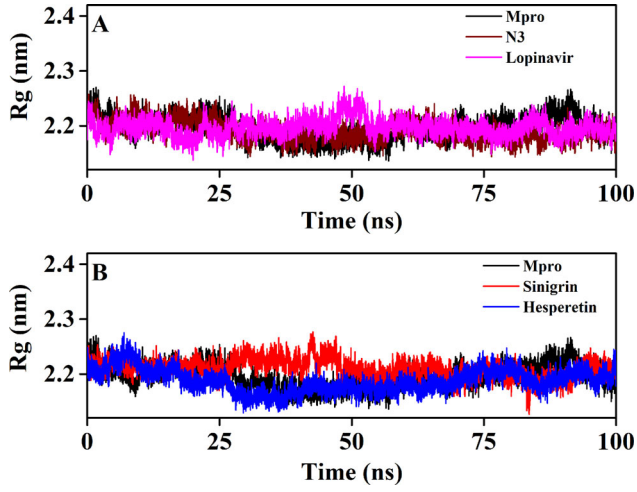

Figure 8. The Rg plots of unligated Mpro and Mpro complexed with two selected standards and *I. indigotica* polyphenols. The Rg plots of unligated Mpro, Mpro-N3 and Mpro-lopinavir complexes are plotted in A while B represents the Rg plots of unligated Mpro, Mpro-sinigrin complex and Mpro-hesperetin complex. The MD simulations for each system were performed for 100 ns.

Table 4. Average values of the Rg and SASA or the simulated systems.

System	Rg (nm)	SASA (nm^2)
Unligated Mpro	2.195	151.4483
Mpro-N3	2.191	155.398
Mpro-lopinavir	2.196	151.2825
Mpro-sinigrin	2.209	151.9689
Mpro-hesperetin	2.187	150.2252

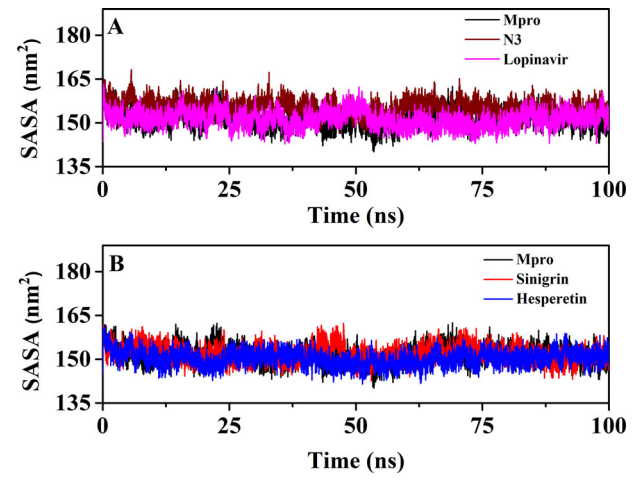

Figure 9. The SASA plots of unligated Mpro and Mpro complexed with selected standards and *I. indigotica* polyphenols. The SASA plots of unligated Mpro, Mpro-N3 and Mpro-lopinavir complexes are plotted in A while B represents the SASA plots of unligated Mpro, Mpro-sinigrin complex and Mpro-hesperetin complex. The MD simulations for each system were performed for 100 ns.

domain III. In the case of unligated Mpro system, most of the amino acid residues within the domain I and II of this system had RMSF fluctuation below 0.3 nm (Figure 7A and B). Only residues 45-60 pertaining to this system experienced higher fluctuations (up to ~0.6 nm). The RMSF plot of the Mpro-N3 complex reflected that very few amino acid residues within domain I, II and III have an RMSF value of more than 0.25 nm (Figure 7A). Interestingly, the RMSF values of several stretches within these three domains of this system (residues 132-138 and 177-195) were more compared to that of unligated system. The Mpro-lopinavir system experienced more or less similar conformational fluctuations to that of unligated Mpro system (Figure 7A). The fluctuationsfor many amino acid residues of domain I were reduced upon the binding of lopinavir to Mpro. Upon analyzing all the RMSF profiles, it was clearly observed that Mpro-sinigrin and Mpro-hesperetin complexes showed lower fluctuations (throughout

Table 5. MM-GBSA values of Mpro-N3, Mpro-lopinavir and two Mpro-polyphenol complexes.

System	Binding Free Energy (kcal/mol)
Mpro-N3	−56.02
Mpro-lopinavir	−40.39
Mpro-sinigrin	−41.75
Mpro-hesperetin	−44.05

all of the domains) as compared to that of unligated Mpro and Mpro-N3/lopinavir complexes (Figure 7B). Many key amino acid residues in the catalytic site of Mpro (especially His41 and Cys145) were significantly reduced after binding to these two polyphenols. The average RMSF values of unligated Mpro, Mpro-N3, Mpro-lopinavir, Mpro-sinigrin, Mpro-hesperetin complexes are ∼0.194 nm, 0.158 nm, ∼0.195 nm, ∼0.131 nm, ∼0.123 nm, respectively (Table 3). These values clearly suggested that Mpro-sinigrin and Mpro-hesperetin complexes experienced less conformational fluctuations than that of Mpro-N3/Mpro-lopinavir complex.

3.3.2. Rg and SASA analysis

We have also estimated the Rg value to assess the compactness of all the complexes (Figure 8 and Table 4). Figure 8A clearly reflected that the Rg values for unligated Mpro, Mpro-N3 and the Mpro-lopinavir complexes over the entire MD simulation was almost identical. The average Rg value for these three systems ranged between 2.191-2.196 nm (Table 4). On the other hand, the average Rg value for Mpro-sinigrin and Mpro-hesperetin systems was 2.209 nm and 2.187 nm, respectively (Table 4). These results suggested that Mpro-sinigrin complex was slightly less compact and Mpro-hesperetin complex was marginally more compact than Mpro-N3/lopinavir complex. SASA values were also calculated to assess the extent of expansion of protein volume in each system (Figure 9 and Table 4). The average SASA values of Mpro-N3 complex

(∼155.398 nm^2) was higher than all the other studied systems suggesting an expansion of Mpro during the interaction with N3. The average SASA values of Mpro-lopinavir, Mpro-sinigrin and Mpro-hesperetin were ∼151.283 nm^2, ∼151.969 nm^2 and ∼150.225 nm^2, respectively (Table 4). These values indicated that Mpro-hesperetin complex experiences less expansion than that of Mpro-lopinavir and Mpro-sinigrin complexes.

3.4. MM-GBSA analysis

The binding free energy of Mpro-sinigrin and Mpro-hesperetin, as well as Mpro-N3 and Mpro-lopinavir, were estimated using MM-GBSA method. The binding free energy values [ΔG_{bind}] of Mpro-N3 and Mpro-lopinavir complexes were found to be −56.02 kcal/mol and −40.39 kcal/mol (Table 5). On the contrary, the ΔG_{bind} values for Mpro-sinigrin, and Mpro-hesperetin complexes, were −41.75 kcal/mol and −44.05 kcal/mol, respectively (Table 5).

MM-GBSA analysis revealed that the binding free energy of 'Mpro-sinigrin interaction' and 'Mpro-hesperetin interaction' is higher than the 'Mpro-lopinavir interaction'. The higher MM-GBSA value (ΔG_{bind}) in the case of Mpro-sinigrin and Mpro-hesperetin is mostly contributed by the SASA and coulombic interactions. Altogether, it can be concluded from these findings that these two polyphenols may be more effective SARS CoV-2 Mpro inhibitors than the previously recommended repurposed drug (lopinavir).

4. Conclusion

In search of new antiviral agents to treat COVID-19, we decided to work with eight polyphenols of *Isatis indigotica*, which were potent SARS CoV-1 Mpro inhibitors. Among them, four polyphenols (indigo, sinigrin, hesperetin and daidzein) were found to be safe for human use based on their pharmacokinetic properties. We tested the inhibition potency of these four polyphenols against SARS CoV-2 Mpro using a computational approach. We conducted molecular docking studies to compare their binding affinities (towards Mpro) with two well-known Mpro inhibitors (N3 and lopinavir). Only two of them (sinigrin and hesperetin) had higher binding affinities than the N3 and lopinavir. Their interaction with both the key catalytic residues (His41 and Cys145) of Mpro was also evidenced. MD trajectories corresponding to these two Mpro-polyphenol complexes and three other systems [unligated Mpro, Mpro-N3 and Mpro-lopinavir] were further analyzed with the aid of RMSD, RMSF, Rg and SASA. These analyses revealed that these two Mpro-polyphenol complexes are highly stable and suffer less conformational fluctuations than that of the Mpro-N3/lopinavir complex. The Mpro-hesperetin system was found to be more compact and less expanded compared to that of the Mpro-sinigrin system as well as the Mpro-N3/lopinavir system. The high stability of these two Mpro-polyphenol complexes was reinforced by MM-GBSA analysis. Therefore, it can be suggested that sinigrin and hesperetin could be considered as potential leads in the development of SARS CoV-2 Mpro inhibitors. But thorough experimental studies are required before using these two polyphenols of *Isatis indigotica* as anti-COVID-19 drugs.

Acknowledgements

RG acknowledges IIT Bhubaneswar for providing fellowship. The authors thank IIT Delhi HPC facility for computational resources.

Disclosure statement

The authors declare that they have no conflicts of interest with the contents of this article.

ORCID

Ayon Chakraborty http://orcid.org/0000-0002-1155-7862

References

Aanouz, I., Belhassan, A., El-Khatabi, K., Lakhlifi, T., El-Ldrissi, M., & Bouachrine, M. (2020). Moroccan Medicinal plants as inhibitors against SARS-CoV-2 main protease: Computational investigations. *Journal of*

Biomolecular Structure and Dynamics, 1–9. https://doi.org/10.1080/07391102.2020.1758790

Abraham, M. J., Murtola, T., Schulz, R., Páll, S., Smith, J. C., Hess, B., & Lindahl, E. (2015). GROMACS: High performance molecular simulations through multi-level parallelism from laptops to supercomputers. *SoftwareX*, *1-2*, 19–25. https://doi.org/10.1016/j.softx.2015.06.001

Anand, K., Ziebuhr, J., Wadhwani, P., Mesters, J. R., & Hilgenfeld, R. (2003). Coronavirus main proteinase (3CLpro) structure: Basis for design of anti-SARS drugs. *Science*, *300*(5626), 1763–1767. https://doi.org/10.1126/science.1085658

Andersen, D. O., Weber, N. D., Wood, S. G., Hughes, B. G., Murray, B. K., & North, J. A. (1991). In vitro virucidal activity of selected anthraquinones and anthraquinone derivatives. *Antiviral Research*, *16*(2), 185–196. https://doi.org/10.1016/0166-3542(91)90024-L

Arun, K. G., Sharanya, C. S., Abhithaj, J., Francis, D., & Sadasivan, C. (2020). Drug repurposing against SARS-CoV-2 using E-pharmacophore based virtual screening, molecular docking and molecular dynamics with main protease as the target. *Journal of Biomolecular Structure and Dynamics*, 1–12. https://doi.org/10.1080/07391102.2020.1779819

Beck, B. R., Shin, B., Choi, Y., Park, S., & Kang, K. (2020). Predicting commercially available antiviral drugs that may act on the novel coronavirus (SARS-CoV-2) through a drug-target interaction deep learning model. *Computational and Structural Biotechnology Journal*, *18*, 784–790. https://doi.org/10.1016/j.csbj.2020.03.025

Berendsen, H. J. C., Postma, J. P. M., Gunsteren, W. F. v., DiNola, A., & Haak, J. R. (1984). Molecular dynamics with coupling to an external bath. *The Journal of Chemical Physics*, *81*(8), 3684–3690. https://doi.org/10.1063/1.448118

Bhardwaj, V. K., Singh, R., Sharma, J., Rajendran, V., Purohit, R., & Kumar, S. (2020). Identification of bioactive molecules from tea plant as SARS-CoV-2 main protease inhibitors. *Journal of Biomolecular Structure and Dynamics*, 1–10. https://doi.org/10.1080/07391102.2020.1766572

Biovia, D. S. (2017). Discovery studio modeling environment. Release.

Borkotoky, S., & Banerjee, M. (2020). A computational prediction of SARS-CoV-2 structural protein inhibitors from Azadirachta indica (Neem). *Journal of Biomolecular Structure and Dynamics*, 1–17. https://doi.org/10.1080/07391102.2020.1774419

Chang, S. J., Chang, Y. C., Lu, K. Z., Tsou, Y. Y., & Lin, C. W. (2012). Antiviral activity of *Isatis indigotica* extract and its derived indirubin against Japanese encephalitis virus. *Evidence-Based Complementary and Alternative Medicine*, *2012*, 925830. https://doi.org/10.1155/2012/925830

Chen, J. (2016). Drug resistance mechanisms of three mutations V32I, I47V and V82I in HIV-1 protease toward inhibitors probed by molecular dynamics simulations and binding free energy predictions. *RSC Advances*, *6*(63), 58573–58585. https://doi.org/10.1039/C6RA09201B

Chen, J., Wang, X., Zhu, T., Zhang, Q., & Zhang, J. Z. (2015). A comparative insight into amprenavir resistance of mutations V32I, G48V, I50V, I54V, and I84V in HIV-1 protease based on thermodynamic integration and MM-PBSA methods. *Journal of Chemical Information and Modeling*, *55*(9), 1903–1913. https://doi.org/10.1021/acs.jcim.5b00173

Chen, N., Zhou, M., Dong, X., Qu, J., Gong, F., Han, Y., Qiu, Y., Wang, J., Liu, Y., Wei, Y., Xia, J., Yu, T., Zhang, X., & Zhang, L. (2020). Epidemiological and clinical characteristics of 99 cases of 2019 novel coronavirus pneumonia in Wuhan, China: A descriptive study. *Lancet*, *395*(10223), 507–513. https://doi.org/10.1016/S0140-6736(20)30211-7

Chou, K. C., Wei, D. Q., & Zhong, W. Z. (2003). Binding mechanism of coronavirus main proteinase with ligands and its implication to drug design against SARS. *Biochemical and Biophysical Research Communications*, *308*(1), 148–151. https://doi.org/10.1016/S0006-291X(03)01342-1

Daina, A., Michielin, O., & Zoete, V. (2017). SwissADME: A free web tool to evaluate pharmacokinetics, drug-likeness and medicinal chemistry friendliness of small molecules. *Scientific Reports*, *7*, 42717. https://doi.org/10.1038/srep42717

Das, B. K., Pv, P., & Chakraborty, D. (2019). Computational insights into factor affecting the potency of diaryl sulfone analogs as Escherichia coli dihydropteroate synthase inhibitors. *Computational Biology and Chemistry*, *78*, 37–52. https://doi.org/10.1016/j.compbiolchem.2018.11.005

Das, S., Sarmah, S., Lyndem, S., & Singha Roy, A. (2020). An investigation into the identification of potential inhibitors of SARS-CoV-2 main protease using molecular docking study. *Journal of Biomolecular Structure and Dynamics*, 1–11. https://doi.org/10.1080/07391102.2020.1763201

Elmezayen, A. D., Al-Obaidi, A., Sahin, A. T., & Yelekci, K. (2020). Drug repurposing for coronavirus (COVID-19): In silico screening of known drugs against coronavirus 3CL hydrolase and protease enzymes. *Journal of Biomolecular Structure and Dynamics*, 1–13. https://doi.org/10.1080/07391102.2020.1758791

Enmozhi, S. K., Raja, K., Sebastine, I., & Joseph, J. (2020). Andrographolide as a potential inhibitor of SARS-CoV-2 main protease: An in silico approach. *Journal of Biomolecular Structure and Dynamics*, 1–7. https://doi.org/10.1080/07391102.2020.1760136

Essmann, U., Perera, L., Berkowitz, M. L., Darden, T., Lee, H., & Pedersen, L. G. (1995). A smooth particle mesh Ewald method. *The Journal of Chemical Physics*, *103*(19), 8577–8593. https://doi.org/10.1063/1.470117

Fan, K., Wei, P., Feng, Q., Chen, S., Huang, C., Ma, L., Lai, B., Pei, J., Liu, Y., Chen, J., & Lai, L. (2004). Biosynthesis, purification, and substrate specificity of severe acute respiratory syndrome coronavirus 3C-like proteinase. *The Journal of Biological Chemistry*, *279*(3), 1637–1642. https://doi.org/10.1074/jbc.M310875200

Frisch, M., Clemente, F., Frisch, M. J., Trucks, G. W., Schlegel, H. B., Scuseria, G. E., Robb, M. A., Cheeseman, J. R., Scalmani, G., Barone, V., Mennucci, B., Petersson, G. A., Nakatsuji, H., Caricato, M., Li, X., Hratchian, H. P., Izmaylov, A. F., Bloino, J., & Zhe, G. (2009). Gaussian 09, Revision A. 01.

Ghosh, R., Chakraborty, A., Biswas, A., & Chowdhuri, S. (2020a). Evaluation of green tea polyphenols as novel corona virus (SARS CoV-2) main protease (Mpro) inhibitors - an in silico docking and molecular dynamics simulation study. *Journal of Biomolecular Structure and Dynamics*, 1–13. https://doi.org/10.1080/07391102.2020.1779818

Ghosh, R., Chakraborty, A., Biswas, A., & Chowdhuri, S. (2020b). Identification of polyphenols from Broussonetia papyrifera as SARS CoV-2 main protease inhibitors using in silico docking and molecular dynamics simulation approaches. *Journal of Biomolecular Structure and Dynamics*, 1–14. https://doi.org/10.1080/07391102.2020.1802347

Gyebi, G. A., Ogunro, O. B., Adegunloye, A. P., Ogunyemi, O. M., & Afolabi, S. O. (2020). Potential inhibitors of coronavirus 3-chymotrypsin-like protease (3CL(pro)): An in silico screening of alkaloids and terpenoids from African medicinal plants. *Journal of Biomolecular Structure and Dynamics*, 1–13. https://doi.org/10.1080/07391102.2020.1764868

Heredia, A., Davis, C., Bamba, D., Le, N., Gwarzo, M. Y., Sadowska, M., Gallo, R. C., & Redfield, R. R. (2005). Indirubin-3′-monoxime, a derivative of a Chinese antileukemia medicine, inhibits P-TEFb function and HIV-1 replication. *AIDS*, *19*(18), 2087–2095. https://doi.org/10.1097/01.aids.0000194805.74293.11

Hertel, L., Chou, S., & Mocarski, E. S. (2007). Viral and cell cycle-regulated kinases in cytomegalovirus-induced pseudomitosis and replication. *PLoS Pathogens*, *3*(1), e6. https://doi.org/10.1371/journal.ppat.0030006

Hess, B., Bekker, H., Berendsen, H. J. C., & Fraaije, J. G. E. M. (1997). LINCS: A linear constraint solver for molecular simulations. *Journal of Computational Chemistry*, *18*(12), 1463–1472. https://doi.org/10.1002/(SICI)1096-987X(199709)18:12<1463::AID-JCC4>3.0.CO;2-H

Hou, T., Wang, J., Li, Y., & Wang, W. (2011). Assessing the performance of the MM/PBSA and MM/GBSA methods. 1. The accuracy of binding free energy calculations based on molecular dynamics simulations. *Journal of Chemical Information and Modeling*, *51*(1), 69–82. https://doi.org/10.1021/ci100275a

Hsu, M. F., Kuo, C. J., Chang, K. T., Chang, H. C., Chou, C. C., Ko, T. P., Shr, H. L., Chang, G. G., Wang, A. H., & Liang, P. H. (2005). Mechanism of the maturation process of SARS-CoV 3CL protease. *The Journal of Biological Chemistry*, *280*(35), 31257–31266. https://doi.org/10.1074/jbc.M502577200

Hsuan, S. L., Chang, S. C., Wang, S. Y., Liao, T. L., Jong, T. T., Chien, M. S., Lee, W. C., Chen, S. S., & Liao, J. W. (2009). The cytotoxicity to leukemia cells and antiviral effects of Isatis indigotica extracts on pseudorabies virus. *Journal of Ethnopharmacology*, *123*(1), 61–67. https://doi.org/10.1016/j.jep.2009.02.028

Islam, R., Parves, M. R., Paul, A. S., Uddin, N., Rahman, M. S., Mamun, A. A., Hossain, M. N., Ali, M. A., & Halim, M. A. (2020). A molecular modeling approach to identify effective antiviral phytochemicals against the main protease of SARS-CoV-2. *Journal of Biomolecular Structure and Dynamics*, 1–12. https://doi.org/10.1080/07391102.2020.1761883

Jin, Z., Du, X., Xu, Y., Deng, Y., Liu, M., Zhao, Y., Zhang, B., Li, X., Zhang, L., Peng, C., Duan, Y., Yu, J., Wang, L., Yang, K., Liu, F., Jiang, R., Yang, X., You, T., Liu, X., … Yang, H. (2020). Structure of M(pro) from SARS-CoV-2 and discovery of its inhibitors. *Nature*, *582*(7811), 289–293. https://doi.org/10.1038/s41586-020-2223-y

Joshi, R. S., Jagdale, S. S., Bansode, S. B., Shankar, S. S., Tellis, M. B., Pandya, V. K., Chugh, A., Giri, A. P., & Kulkarni, M. J. (2020). Discovery of potential multi-target-directed ligands by targeting host-specific SARS-CoV-2 structurally conserved main protease. *Journal of Biomolecular Structure and Dynamics*, 1–16. https://doi.org/10.1080/07391102.2020.1760137

Kandeel, M., & Al-Nazawi, M. (2020). Virtual screening and repurposing of FDA approved drugs against COVID-19 main protease. *Life Sciences*, *251*, 117627. https://doi.org/10.1016/j.lfs.2020.117627

Khan, R. J., Jha, R. K., Amera, G. M., Jain, M., Singh, E., Pathak, A., Singh, R. P., Muthukumaran, J., & Singh, A. K. (2020). Targeting SARS-CoV-2: A systematic drug repurposing approach to identify promising inhibitors against 3C-like proteinase and 2′-O-ribose methyltransferase. *Journal of Biomolecular Structure and Dynamics*, 1–14. https://doi.org/10.1080/07391102.2020.1753577

Kim, H. K., Jeon, W. K., & Ko, B. S. (2001). Flavanone glycosides from Citrus junos and their anti-influenza virus activity. *Planta Medica*, *67*(6), 548–549. https://doi.org/10.1055/s-2001-16484

Kim, Y., Liu, H., Galasiti Kankanamalage, A. C., Weerasekara, S., Hua, D. H., Groutas, W. C., Chang, K. O., & Pedersen, N. C. (2016). Reversal of the progression of fatal coronavirus infection in cats by a broad-spectrum coronavirus protease inhibitor. *PLoS Pathogens*, *12*(3), e1005531. https://doi.org/10.1371/journal.ppat.1005531

Ko, H. C., Wei, B. L., & Chiou, W. F. (2006). The effect of medicinal plants used in Chinese folk medicine on RANTES secretion by virus-infected human epithelial cells. *Journal of Ethnopharmacology*, *107*(2), 205–210. https://doi.org/10.1016/j.jep.2006.03.004

Lin, C. W., Tsai, F. J., Tsai, C. H., Lai, C. C., Wan, L., Ho, T. Y., Hsieh, C. C., & Chao, P. D. (2005). Anti-SARS coronavirus 3C-like protease effects of Isatis indigotica root and plant-derived phenolic compounds. *Antiviral Research*, *68*(1), 36–42. https://doi.org/10.1016/j.antiviral.2005.07.002

Macchiagodena, M., Pagliai, M., & Procacci, P. (2020). Identification of potential binders of the main protease 3CL(pro) of the COVID-19 via structure-based ligand design and molecular modeling. *Chemical Physics Letters*, *750*, 137489. https://doi.org/10.1016/j.cplett.2020.137489

Mahanta, S., Chowdhury, P., Gogoi, N., Goswami, N., Borah, D., Kumar, R., Chetia, D., Borah, P., Buragohain, A. K., & Gogoi, B. (2020). Potential anti-viral activity of approved repurposed drug against main protease of SARS-CoV-2: An in silico based approach. *Journal of Biomolecular Structure and Dynamics*, 1–10. https://doi.org/10.1080/07391102.2020.1768902

Mak, N. K., Leung, C. Y., Wei, X. Y., Shen, X. L., Wong, R. N., Leung, K. N., & Fung, M. C. (2004). Inhibition of RANTES expression by indirubin in influenza virus-infected human bronchial epithelial cells. *Biochemical Pharmacology*, *67*(1), 167–174. https://doi.org/10.1016/j.bcp.2003.08.020

Miyamoto, S., & Kollman, P. A. (1992). Settle: An analytical version of the SHAKE and RATTLE algorithm for rigid water models. *Journal of Computational Chemistry*, *13*(8), 952–962. https://doi.org/10.1002/jcc.540130805

Morris, G. M., Huey, R., Lindstrom, W., Sanner, M. F., Belew, R. K., Goodsell, D. S., & Olson, A. J. (2009). AutoDock4 and AutoDockTools4: Automated docking with selective receptor flexibility. *Journal of Computational Chemistry*, *30*(16), 2785–2791. https://doi.org/10.1002/jcc.21256

Morris, G. M., Huey, R., & Olson, A. J. (2008). Using AutoDock for ligand-receptor docking. *Curr Protoc Bioinformatics*, *Chapter 8*, Unit 8 14. https://doi.org/10.1002/0471250953.bi0814s24

Muralidharan, N., Sakthivel, R., Velmurugan, D., & Gromiha, M. M. (2020). Computational studies of drug repurposing and synergism of lopinavir, oseltamivir and ritonavir binding with SARS-CoV-2 protease against COVID-19. *Journal of Biomolecular Structure and Dynamics*, 1–6. https://doi.org/10.1080/07391102.2020.1752802

Odhar, H. A., Ahjel, S. W., Albeer, A., Hashim, A. F., Rayshan, A. M., & Humadi, S. S. (2020). Molecular docking and dynamics simulation of FDA approved drugs with the main protease from 2019 novel coronavirus. *Bioinformation*, *16*(3), 236–244. https://doi.org/10.6026/97320630016236

Oostenbrink, C., Villa, A., Mark, A. E., & van Gunsteren, W. F. (2004). A biomolecular force field based on the free enthalpy of hydration and solvation: The GROMOS force-field parameter sets 53A5 and 53A6. *Journal of Computational Chemistry*, *25*(13), 1656–1676. https://doi.org/10.1002/jcc.20090

Paredes, A., Alzuru, M., Mendez, J., & Rodriguez-Ortega, M. (2003). Anti-Sindbis activity of flavanones hesperetin and naringenin. *Biological & Pharmaceutical Bulletin*, *26*(1), 108–109. https://doi.org/10.1248/bpb.26.108

Parrinello, M., & Rahman, A. (1981). Polymorphic transitions in single crystals: A new molecular dynamics method. *Journal of Applied Physics*, *52*(12), 7182–7190. https://doi.org/10.1063/1.328693

Pires, D. E., Blundell, T. L., & Ascher, D. B. (2015). pkCSM: Predicting small-molecule pharmacokinetic and toxicity properties using graph-based signatures. *Journal of Medicinal Chemistry*, *58*(9), 4066–4072. https://doi.org/10.1021/acs.jmedchem.5b00104

Ren, L. L., Wang, Y. M., Wu, Z. Q., Xiang, Z. C., Guo, L., Xu, T., Jiang, Y. Z., Xiong, Y., Li, Y. J., Li, X. W., Li, H., Fan, G. H., Gu, X. Y., Xiao, Y., Gao, H., Xu, J. Y., Yang, F., Wang, X. M., Wu, C., … Wang, J. W. (2020). Identification of a novel coronavirus causing severe pneumonia in human: A descriptive study. *Chinese Medical Journal*, *133*(9), 1015–1024. https://doi.org/10.1097/CM9.0000000000000722

Rota, P. A., Oberste, M. S., Monroe, S. S., Nix, W. A., Campagnoli, R., Icenogle, J. P., Penaranda, S., Bankamp, B., Maher, K., Chen, M. H., Tong, S., Tamin, A., Lowe, L., Frace, M., DeRisi, J. L., Chen, Q., Wang, D., Erdman, D. D., Peret, T. C., … Bellini, W. J. (2003). Characterization of a novel coronavirus associated with severe acute respiratory syndrome. *Science*, *300*(5624), 1394–1399. https://doi.org/10.1126/science.1085952

Sanche, S., Lin, Y. T., Xu, C., Romero-Severson, E., Hengartner, N., & Ke, R. (2020). High contagiousness and rapid spread of severe acute respiratory syndrome coronavirus 2. *Emerging Infectious Diseases*, *26*(7), 1470–1477. https://doi.org/10.3201/eid2607.200282

Schuttelkopf, A. W., & van Aalten, D. M. (2004). PRODRG: A tool for high-throughput crystallography of protein-ligand complexes. *Acta Crystallographica. Section D, Biological Crystallography*, *60*(Pt 8), 1355–1363. https://doi.org/10.1107/S0907444904011679

Semple, S. J., Pyke, S. M., Reynolds, G. D., & Flower, R. L. (2001). In vitro antiviral activity of the anthraquinone chrysophanic acid against poliovirus. *Antiviral Research*, *49*(3), 169–178. https://doi.org/10.1016/S0166-3542(01)00125-5

Tahir Ul Qamar, M., Alqahtani, S. M., Alamri, M. A., & Chen, L. L. (2020). Structural basis of SARS-CoV-2 3CL(pro) and anti-COVID-19 drug discovery from medicinal plants. *Journal of Pharmaceutical Analysis*, *10*(4), 313–319. https://doi.org/10.1016/j.jpha.2020.03.009

Tang, B., Bragazzi, N. L., Li, Q., Tang, S., Xiao, Y., & Wu, J. (2020). An updated estimation of the risk of transmission of the novel coronavirus (2019-nCov). *Infectious Disease Modelling*, *5*, 248–255. https://doi.org/10.1016/j.idm.2020.02.001

Toyoshima, Y., Nemoto, K., Matsumoto, S., Nakamura, Y., & Kiyotani, K. (2020). SARS-CoV-2 genomic variations associated with mortality rate of COVID-19. *Journal of Human Genetics*, *65*(12), 1075–1082. https://doi.org/10.1038/s10038-020-0808-9

Umesh, K. D., Selvaraj, C., Singh, S. K., & Dubey, V. K. (2020). Identification of new anti-nCoV drug chemical compounds from Indian spices exploiting SARS-CoV-2 main protease as target. *Journal of Biomolecular Structure and Dynamics*, 1–9. https://doi.org/10.1080/07391102.2020.1763202

Zheng, J. (2020). SARS-CoV-2: An emerging coronavirus that causes a global threat. *International Journal of Biological Sciences*, *16*(10), 1678–1685. https://doi.org/10.7150/ijbs.45053

Zhu, N., Zhang, D., Wang, W., Li, X., Yang, B., Song, J., Zhao, X., Huang, B., Shi, W., Lu, R., Niu, P., Zhan, F., Ma, X., Wang, D., Xu, W., Wu, G., Gao, G. F., Tan, W., & China Novel Coronavirus Investigating and Research Team. (2020). A novel coronavirus from patients with pneumonia in China, 2019. *The New England Journal of Medicine*, *382*(8), 727–733. https://doi.org/10.1056/NEJMoa2001017

Zou, P., & Koh, H. L. (2007). Determination of indican, isatin, indirubin and indigotin in Isatis indigotica by liquid chromatography/electrospray ionization tandem mass spectrometry. *Rapid Communications in Mass Spectrometry*, *21*(7), 1239–1246. https://doi.org/10.1002/rcm.2954